

# Dynamics of topological solitons in two-dimensional ferromagnets

Denis D. Sheka<sup>1</sup>, Christian Schuster<sup>2</sup>, Boris A. Ivanov<sup>3</sup>,  
and Franz G. Mertens<sup>2</sup>

<sup>1</sup> National Taras Shevchenko University of Kiev, 03127 Kiev, Ukraine

<sup>2</sup> Physics Institute, University of Bayreuth, 95440 Bayreuth, Germany

<sup>3</sup> Institute of Magnetism, 04071 Kiev, Ukraine

E-mail: Denis\_Sheka@univ.kiev.ua

## Abstract.

Dynamical topological solitons are studied in classical two-dimensional Heisenberg easy-axis ferromagnets. The properties of such solitons are treated both analytically in the continuum limit and numerically by spin dynamics simulations of the discrete system. Excitation of internal mode causes orbital motion. This is confirmed by simulations.

Submitted to: *J. Phys.: Condens. Matter*

PACS numbers: 75.10.Hk, 75.30.Ds, 05.45.-a

Dated: 6 March 2019

## 1. Introduction

The analysis of 2D magnetic solitons continues for more than 25 years, for reviews see Refs. [1, 2, 3]. Such solitons are well-known to play an important role in the physics of 2D magnetic systems. In easy-plane magnets with continuously degenerated ground state there appear magnetic vortices, which are responsible for the Berezinskiĭ–Kosterlitz–Thouless phase transition [4, 5]. The presence of vortices leads to the emergence of central peaks in dynamical response functions of the magnet [6], which can be observed experimentally [7, 8, 9, 10, 11]. Belavin and Polyakov were the first who constructed exact analytical solutions for 2D topological solitons in the *isotropic* magnet in the continuum limit, and proved that such solitons are responsible for the destruction of the long-range ordering for finite temperature [12]. Topological solitons also exist for the *anisotropic* magnets. In easy-axis magnets with discrete degenerated ground state vortices are absent, but there appear various types of localized topological solitons. The signature of such solitons in the response functions was observed experimentally [13, 14, 15, 16, 17]; for a review of EPR detection of solitons see Ref. [18]. The structure of topological solitons in the continuum approximation was studied in detail, it is described by a topologically nontrivial distribution of the magnetization field  $\mathbf{m}(\mathbf{r}, t)$  [1].

The basic problem arising in the soliton physics of two-dimensional magnets is related with the stability of solitons. According to the Hobart–Derrick theorem [19, 20], stable static non-one-dimensional solitons with finite energy and finite radius do not exist for the standard models of nonlinear field theory; the soliton is unstable against collapse. Specifically, this is true for uniaxial two-dimensional ferromagnets with an anisotropy energy density of the form  $W_a \propto m_x^2 + m_y^2$ . One possibility to construct stable non-one-dimensional solitons is connected with the presence of additional integrals of motion, whose values do not vanish in the static limit [1, 21]. For example, such solitons can be realized for the uniaxial ferromagnet due to the conservation of the  $z$ -projection  $S_z$  of the total spin [1, 21] or the  $z$ -projection  $L_z$  of the orbital angular momentum of the magnetization field [22, 23]. This leads to the appearance of *precessional* solitons [1] and *rotational* solitons [22, 23], respectively. The precessional solitons can exist also for the semi-topological case, so-called Q-balls [24, 25, 26]. Precessional solitons are known for a number of models used in field theory and condensed matter physics, see Ref. [27].

The problem of the dynamics of topological solitons in 2D ferromagnets is a complicated task. The general features of 2D soliton and vortex dynamics are not clear at present. The presence of a gyroforce acting on a moving soliton is the only thing which is well established, but the free gyroscopic dynamics has not been reported till now for any 2D solitons. For the easy-plane magnets the weak localization of the vortex is related to the gapless magnon spectrum; hence the vortex dynamics is strongly coupled to a “cloud” of magnons, and the boundary effects become decisive for a finite system. As a result, computer simulations of magnetic vortex dynamics in a large but finite lattice show a motion which can be described by complicated non-Newtonian dynamical equations with nonlocal terms [28]. The origin of such terms is not clear at present, in particular they appear either due to the weak localization of the vortex structure or due to the strong coupling of the vortex motion with magnons. For the isotropic magnet numerical analysis shows the absence of soliton motion [29]. Again, as for the vortices of easy-plane systems, the dynamics of Belavin–Polyakov solitons is not localized due to the gapless magnon dispersion law.

A very attractive candidate to discuss the general problems of the soliton motion in models like ferromagnet, where Lorentz and Galilean invariance are absent, is the easy-axis ferromagnet. In this case the soliton shape is exponentially localized. It seems to be possible to separate the soliton motion from the magnons due to their finite activation energy, hence an effective soliton dynamics should have usual particle-like properties, which are characterized by a finite soliton mass. At the same time the movement of the soliton in the non-Lorentz invariant model breaks the symmetry of the soliton structure, which makes difficulties in studying its evolution. The first attempt to analyze the 2D topological soliton dynamics was made in Ref. [30], where a free rotational motion was predicted. It results in a finite mass for the small-radius soliton [30], while the mass of the localized soliton diverges as the logarithm of the system size according to [16]. A detailed analysis of the dynamics of linear magnon modes around the soliton was performed in Ref. [31], where the topological soliton in easy-axis ferromagnets was shown to have a set of internal modes. Such truly local modes strongly influence the dynamics of the soliton. Using linear analysis we have predicted in [31] a possible inertial motion of the soliton. Thus it is of interest to analyze the soliton motion using spin dynamics simulations on a finite lattice.

The present work is devoted to the analysis of the dynamical properties of topological solitons in easy-axis ferromagnets, both in the discrete model with weak anisotropy and in the continuum model. We should stress here that topological solitons were studied only in the frameworks of continuum field approaches in all above mentioned papers. As far as we know spin dynamics simulations for 2D topological solitons were performed only in [32], where large radius solitons were considered, and *no* motion of a soliton as a whole was seen: in all simulations the soliton center of mass did not move. However, the topological small radius solitons become interesting now due to possible applications in high-energy physics [33] and the quantum Hall effect [34]. In 2D magnets such solitons are interesting due to possible mobility and therefore inertial properties. In this paper we perform spin dynamics simulations for a wide range of soliton shapes: from large radius solitons to small ones. Hence the soliton dynamics is very sensitive to the spin field perturbations, we first revise the problem of centrosymmetric precessional solitons both analytically and numerically. The main issue is to move the soliton. For vortices, the motion appears because of the influence of the system border. In the case of Lorentz-invariant models, like the  $\sigma$ -model for antiferromagnets, it is enough to set up an initial distribution of the sublattice magnetization field  $\mathbf{l}(\mathbf{r}, 0)$  and its time derivative  $\partial_t \mathbf{l}(\mathbf{r}, 0)$ . However for the ferromagnet, which is described by a first-order equation with respect to time, the effect of dynamics is only the deformation of the soliton shape. One can expect to excite the motion using some relevant deformation of the initial soliton shape; the point is to find and set up the initial spin distribution  $\mathbf{m}(\mathbf{r}, 0)$ , which provides the motion. We will move the soliton by exciting internal modes, which results in perfect orbital motion of the soliton.

## 2. Discrete Model and Continuum Limit for 2D Ferromagnets

We consider the simplest model of the classical 2D ferromagnet described by the following Hamiltonian

$$\mathcal{H} = -\frac{J}{2} \sum_{\langle \mathbf{n}, \boldsymbol{\alpha} \rangle} (\mathbf{S}_{\mathbf{n}} \cdot \mathbf{S}_{\mathbf{n}+\boldsymbol{\alpha}} + \delta S_{\mathbf{n}}^z S_{\mathbf{n}+\boldsymbol{\alpha}}^z). \quad (1)$$

Here  $\mathbf{S}_n \equiv (S_n^x, S_n^y, S_n^z)$  is a classical spin vector with fixed length  $S$  (in units of the Plank constant  $\hbar$ ) on the site  $\mathbf{n}$  of a two-dimensional square lattice,  $\boldsymbol{\alpha}$  is a vector to a nearest neighbor. The model includes the isotropic Heisenberg exchange interaction,  $J > 0$  is the exchange integral, and the spatially homogeneous uniaxial exchange anisotropy,  $\delta$  is the anisotropy constant. The summation runs over nearest-neighbor pairs  $(\mathbf{n}, \mathbf{n} + \boldsymbol{\alpha})$ . The case  $\delta = 0$  corresponds to the isotropic model. To describe the anisotropy effects we will consider the case when  $\delta > 0$ , then the  $z$ -axis suppose the easiest magnetization.

The spin dynamics is described by the discrete version of the Landau–Lifshitz equations

$$\frac{d\mathbf{S}_n}{dt} = -\frac{1}{\hbar} \left[ \mathbf{S}_n \times \frac{\partial \mathcal{H}}{\partial \mathbf{S}_n} \right]. \quad (2)$$

The model of the pure uniaxial ferromagnet has well-known linear excitations (magnons) above the ground state  $\mathbf{S}_n^z = 1$  of the form  $1 - \mathbf{S}_n^z = \text{const} \ll 1$ ,  $\mathbf{S}_n^x + i\mathbf{S}_n^y \propto \exp(ik_x a + ik_y a - i\omega t)$ , which have the finite gap dispersion law

$$\omega(\mathbf{k}) = \omega_0 + \frac{4JS}{\hbar} \left[ \sin^2 \left( \frac{k_x a}{2} \right) + \sin^2 \left( \frac{k_y a}{2} \right) \right]. \quad (3)$$

Here  $\omega_0 = 4JS\delta/\hbar$  is the homogeneous ferromagnetic resonance frequency,  $\mathbf{k}$  is the wave vector.

In the case of weak anisotropy,  $\delta \ll 1$ , the characteristic size  $l_0 = a/\sqrt{4\delta}$  of the excitations is larger than the lattice constant  $a$ , so that in the lowest approximation in the small parameter  $a/l_0$  and with weak gradients of magnetization one can use the continuum approximation for the Hamiltonian (1) by introducing the normalized spin  $\mathbf{s} = \mathbf{S}/S = (\sin \theta \cos \phi; \sin \theta \sin \phi; \cos \theta)$ . The continuum version of the Hamiltonian is

$$\mathcal{E}[\theta, \phi] = \frac{JS^2}{2} \int d^2x \left[ (\nabla \theta)^2 + \sin^2 \theta (\nabla \phi)^2 + \frac{\sin^2 \theta}{l_0^2} + a^2 \Delta W \right], \quad (4)$$

where  $\Delta W$  schematically represents the terms with higher derivatives, which have a complicated structure and whose concrete form will not be used. In terms of the fields  $\theta$  and  $\phi$ , the Landau–Lifshitz equations (2) read

$$\sin \theta \partial_t \phi = -\frac{a^2}{\hbar S} \frac{\delta \mathcal{E}}{\delta \theta}, \quad \sin \theta \partial_t \theta = \frac{a^2}{\hbar S} \frac{\delta \mathcal{E}}{\delta \phi}. \quad (5)$$

In the longwavelength limit the magnon excitations of the form  $\theta = \text{const} \ll 1$ ,  $\phi = \mathbf{k} \cdot \mathbf{r} - \omega t$ , have the following dispersion law,

$$\omega(\mathbf{k}) = \omega_0(1 + k^2 l_0^2), \quad (6)$$

which follows from (3) in the lowest approximation in  $ka \ll 1$ . Note that higher gradients like  $(\nabla \mathbf{s})^4$ , which are not so important for magnons, could be relevant for the solitons, see below.

### 3. The Fate of the Belavin–Polyakov Soliton

The simplest nonlinear excitation of the model (5) is a 2D soliton, which has a finite energy. Such a soliton is characterized by a homogeneous distribution of the magnetization far from the soliton. The topological properties of the soliton are determined by the mapping of the  $xy$ -plane to the  $S^2$ -sphere of the order parameter

space. This mapping is described by the homotopic group  $\pi_2(S^2) = \mathbb{Z}$ , which is characterized by the topological invariant (Pontryagin index)

$$q = \frac{1}{8\pi} \int d^2x \varepsilon_{\alpha\beta} [\mathbf{m} \cdot (\nabla_\alpha \mathbf{m} \times \nabla_\beta \mathbf{m})] = \frac{1}{4\pi} \int \sin \theta d\theta d\phi. \quad (7)$$

The Pontryagin index takes integer values,  $q \in \mathbb{Z}$ , being an integral of motion.

To understand the structure of the topological soliton, let us consider the case of a pure isotropic magnet (the model (4), (5) without anisotropy and the term  $\Delta W$ ) with an exact analytical solution, the so-called Belavin–Polyakov soliton of the form [12]

$$\tan \frac{\theta}{2} = \left( \frac{R}{r} \right)^{|q|}, \quad \phi = \varphi_0 + q\chi, \quad (8)$$

where  $r$  and  $\chi$  are polar coordinates in the  $XY$ -plane,  $\varphi_0$  is an arbitrary constant. The energy (4) of this soliton does not depend on its radius  $R$  due to the scale invariance of the isotropic model,  $\mathcal{E} = 4\pi|q|JS^2$ , see Ref. [12]. The soliton solutions of Belavin–Polyakov-type now are a perspective for the quantum Hall effect, where they could play the role of low-energy charged excitations [35]. At the same time the Belavin–Polyakov solitons seem to be a rather academic problem for the 2D magnets, because all real magnets have some anisotropy. Even small anisotropy breaks the scale invariance of the model (there appears the natural scale  $l_0$ ); the soliton energy in the lowest approximation in  $R/l_0$  is equal to

$$\mathcal{E} = 4\pi|q|JS^2 + \text{const} \left( \frac{R}{l_0} \right)^2. \quad (9)$$

This expression for the energy does not have a minimum for any finite value of  $R$ , which results in the absence of static soliton solutions. This statement does not depend on the concrete form of the anisotropy term used in the model (4): taking into account any kind of easy-axial anisotropy or the Zeeman energy  $w_H \sim (1 - \cos \theta)H$  in an external field  $\mathbf{H} = H\mathbf{e}_z$ , we obtain a soliton energy in a form similar to (9), i. e. proportional to  $R^2$ . The energy has a minimum for  $R = 0$  only.

One can suppose that the anisotropy is very weak (the typical scale  $l_0$  reaches the system size). However, even in such a case the scale invariance is broken when considering the real, discrete model. In the continuum model this corresponds to a term like  $J'S^2a^2 (\nabla^2 \mathbf{m})^2$  in the energy density, which gives a contribution to the soliton energy  $\propto J'S^2a^2/R^2$ . Even without magnetic anisotropy such a term make the soliton collapse for  $J' < 0$ , or leads to a spreading of the soliton onto the whole magnet for  $J' > 0$ .

Note that stable static 2D and 3D solitons can exist in rather exotic models, which contain, e.g., higher powers of field gradients, like  $(\nabla_i \mathbf{m})^4$  (with *positive* sign) [36, 37, 38, 39] together with anisotropic terms. However, for Heisenberg magnets the stabilization of this type is very problematic. In particular, for discrete models of magnets with Heisenberg interactions between nearest neighbors only, i.e. without the consideration of bi-quadratic exchange or next-nearest-neighbors interaction, the coefficient in the term with gradients in the fourth power is *negative*, and this source of soliton stabilization does not work.

Thus, the Belavin–Polyakov case is a “singular” point between the anisotropic models for real magnets: all attempts to consider non-scale-invariant models, either taking into account other types of magnetic anisotropy or discreteness effects via high

derivative terms, lead to the destabilization of the soliton structure. We will consider a different way to stabilize the soliton, taking into account additional integrals of motion. This is the dynamic stabilization of the soliton structure.

#### 4. The Structure of Precessional Soliton

For the pure uniaxial ferromagnet the Hamiltonian (1) does not depend explicitly on the variable  $\phi$  due to the spin-space isotropy (in contrast to the lattice, which is always anisotropic but in coordinate space). This condition corresponds to the additional integral of motion

$$N = \sum_{\mathbf{n}} (S - S_{\mathbf{n}}^z). \quad (10)$$

When  $N \gg 1$  and the WKB approach is valid, one can consider  $N \in \mathbb{N}$  as the number of magnons, bound in the soliton, see Ref. [1]. The conservation law (10) can provide a conditional minimum of the Hamiltonian, which stabilize the possible soliton solution, see below. The continuous version of (10) reads

$$N = \frac{S}{a^2} \int d^2x (1 - \cos \theta). \quad (11)$$

Let us consider the simplest nonlinear excitation for the model (4), (5) with  $\Delta W = 0$ . It is the so-called *centrosymmetric topological precessional soliton*, which has the following structure:

$$\theta = \theta_0(\rho), \quad \phi = \varphi_0 + q\chi - \omega_p t, \quad (12)$$

where  $\rho = r/l_0$  is the dimensionless radius and  $\omega_p \in (0, \omega_0)$  is the frequency of the internal precession. We will discuss only the case  $q = 1$ , when the soliton has a lower energy. The form of the function  $\theta_0(\bullet)$  satisfies the following differential problem:

$$\frac{d^2\theta_0}{d\rho^2} + \frac{1}{\rho} \frac{d\theta_0}{d\rho} - \sin\theta_0 \cos\theta_0 \left(1 + \frac{1}{\rho^2}\right) + \frac{\omega_p}{\omega_0} \sin\theta_0 = 0, \quad (13a)$$

$$\theta_0(0) = \pi, \quad \theta_0(\infty) = 0. \quad (13b)$$

This equation was solved numerically in Refs. [40, 41, 42]. For the case of a centrosymmetric soliton the number of bound magnons

$$N = N_0 \int_0^\infty \rho d\rho [1 - \cos\theta_0(\rho)], \quad (14)$$

where  $N_0 = 2\pi S l_0^2 / a^2$  is the characteristic number of bound magnons for 2D magnets [40]. Note that for a more adequate model with  $\Delta W \neq 0$  the central symmetry is broken and only variational approaches could be applied [43]. Integrating (13a), one can easily obtain the identity

$$\int_0^\infty \sin^2 \theta_0(\rho) \rho d\rho = \frac{2\omega_p}{\omega_0} \int_0^\infty [1 - \cos\theta_0(\rho)] \rho d\rho, \quad (15)$$

which gives a possibility to rewrite the soliton energy (4) as follows

$$\mathcal{E} = \mathcal{E}_{\text{exc}} + \hbar\omega_p N, \quad \mathcal{E}_{\text{exc}} = \frac{JS^2}{2} \int d^2x [(\nabla\theta)^2 + \sin^2\theta (\nabla\phi)^2]. \quad (16)$$

Note that the linear dependence of the soliton energy  $\mathcal{E}$  on  $N$  agrees with the general relation  $\hbar\omega_p = \delta\mathcal{E}/\delta N$ .

The shape of the soliton essentially depends on the number  $N$  of bound magnons. In the case of solitons with large radius  $R$  (equivalent to  $N \gg N_0$ ), the approximate “domain wall” solution works well, see Ref. [1]. This solution has the shape of a curved 1D domain wall at the distance  $R$

$$\cos \theta_0(r) = \tanh \frac{r - R}{l_0}. \quad (17)$$

Using this simple structure one can obtain the number of bound magnons, which is proportional to the area of the soliton,  $N \approx N_0(R/l_0)^2$ , and precession frequency

$$\frac{\omega_p}{\omega_0} \approx \frac{l_0}{R} \approx \sqrt{\frac{N_0}{N}}. \quad (18)$$

In the case of small radius solitons ( $N \ll N_0$ ), the following asymptotically exact solution works well [42]

$$\tan \frac{\theta_0(r)}{2} = \frac{R}{r_0} K_1 \left( \frac{r}{r_0} \right), \quad r_0 = \frac{l_0}{\sqrt{1 - \omega_p/\omega_0}}, \quad (19)$$

where  $K_1(\bullet)$  is the McDonald function. It provides correct behavior for  $r < R \ll l_0$ , where it converts to the Belavin–Polyakov solution (8) and provides a correct exponential decay for  $r \gg R$ . In this case the frequency of the soliton precession  $\omega_p \rightarrow \omega_0$  when  $N \rightarrow 0$ , but the dependence  $\omega_p(N)$  has a singularity at the origin:  $d\omega_p/dN \rightarrow \infty$  as  $N \rightarrow 0$

$$\frac{\omega_p}{\omega_0} \approx 1 - \frac{1}{\ln(8N_0/e\gamma^2 N)}, \quad (20)$$

where  $\gamma \approx 1.78$  is the Euler constant, see Refs. [42, 43].

In the intermediate case of arbitrary  $R$ , it is possible to use an approximate trial function of the form, proposed in Ref. [31],

$$\tan \frac{\theta_0(r)}{2} = \frac{R}{r} \exp \left( -\frac{r - R}{r_0} \right). \quad (21)$$

Here  $R$  is the fitting parameter, which was found in Ref. [31] by fitting the trial function (21) to the numerical solution of the differential problem (4). The value of this fitting parameter is closed to the soliton radius, which satisfies the condition  $\cos \theta_0(R) = 0$ .

The trial function (21) gives a possibility to describe approximately the soliton shape for a given radius  $R$ . However, it contains one extra parameter,  $\omega_p$ , due to the dependence  $r_0 = r_0(\omega_p)$ . One can calculate approximately the  $\omega_p(R)$ -dependence as follows

$$\omega_p(R) \approx \frac{\omega_0 l_0}{R + l_0}, \quad (22)$$

which provides the correct asymptote (18) for  $R \gg l_0$  and gives the limiting value  $\omega_p = 0$  for  $R \ll l_0$ . In the same approach the typical size of the exponential tail of the soliton  $r_0 \approx l_0 \sqrt{(R + l_0)/R}$ ; thus for the soliton shape we have finally

$$\tan \frac{\theta_0(r)}{2} \approx \frac{R}{r} \exp \left( -\frac{r - R}{l_0} \sqrt{\frac{R}{R + l_0}} \right), \quad \phi = \varphi_0 + \chi - \omega_p t. \quad (23)$$

We will use this simple expression as initial condition for our numerical simulations in Sec. 6.

## 5. The Soliton Dynamics

To describe the dynamics of the soliton as a whole, it is necessary first of all to introduce an effective soliton coordinate. Let us define the soliton position  $\mathbf{X}(t) = (X(t), Y(t))$  as the center of mass of the  $z$ -component of the magnetization field:

$$\mathbf{X}(t) = \frac{S}{Na^2} \int d^2x \mathbf{r} (1 - \cos \theta). \quad (24)$$

Using this quantity we will look for the way of possible soliton deformation, which initialize its motion. In order to realize this idea, let us derive the soliton speed

$$\frac{d\mathbf{X}}{dt} = \frac{JS^2}{\hbar N} \int d^2x \sin^2 \theta \nabla \phi. \quad (25)$$

It is convenient to classify all possible perturbations of the soliton shape using a complete set of functions. We choose the solution of the linearized problem, which provides a set of partial waves.

Let us remind that the soliton in an easy-axial ferromagnet has a number of local magnon modes. The existence of local modes is possible because of the gap in the magnon spectrum as predicted in Ref. [31]; such modes correspond to different types of soliton shape oscillations. To describe the local modes one has to linearize the Landau–Lifshitz equations (5) on the soliton background as it was done in Ref. [31]. We use the partial-wave expansion

$$\begin{aligned} \theta &= \theta_0(\rho) + \sum_m A_m f_m(\rho) \cos(m\chi - \omega_m t), \\ \phi &= \varphi_0 + \chi - \omega_p t + \sum_m \frac{A_m}{\sin \theta_0} g_m(\rho) \sin(m\chi - \omega_m t), \end{aligned} \quad (26)$$

where  $\omega_m$  is the magnon frequency in the rotating frame. The radial functions  $f_m(\rho) = u_m(\rho) + v_m(\rho)$  and  $g_m(\rho) = u_m(\rho) - v_m(\rho)$  satisfy the following eigenvalue problem for two coupled Schrödinger-like equations:

$$\begin{aligned} \left[ -\frac{d^2}{d\rho^2} - \frac{1}{\rho} \frac{d}{d\rho} + V_+(\rho) - \frac{\omega_m}{\omega_0} \right] u_m &= W(\rho) v_m, \\ \left[ -\frac{d^2}{d\rho^2} - \frac{1}{\rho} \frac{d}{d\rho} + V_-(\rho) + \frac{\omega_m}{\omega_0} \right] v_m &= W(\rho) u_m, \end{aligned} \quad (27)$$

where the radial “potentials” are

$$\begin{aligned} V_{\pm}(\rho) &= \frac{(\cos \theta_0 \pm m)^2}{\rho^2} + \cos \theta_0 \left( \cos \theta_0 - \frac{\omega_p}{\omega_0} \right) - \frac{1}{2} \sin^2 \theta_0 \left( 1 + \frac{1}{\rho^2} \right) - \frac{1}{2} (\theta'_0)^2, \\ W(\rho) &= \frac{1}{2} \sin^2 \theta_0 \left( 1 + \frac{1}{\rho^2} \right) - \frac{1}{2} (\theta'_0)^2. \end{aligned}$$

The local modes exist in a range of frequencies inside the gap,  $\omega_m^{\text{loc}} \in (0, \omega_0 - \omega_p)$ . The number of local modes essentially depends on the soliton radius: when the soliton radius decreases, the local modes leave the gap range, transforming to the quasi-local modes with singularities in the scattering picture. For the soliton with  $R \leq R_c = 1.52l_0$  there exists only one local mode, namely the mode with  $m = -1$ , and it is this mode which corresponds to the soliton motion.



Let us calculate the soliton velocity (25) using the partial wave ansatz (26). In the linear approximation in  $A_m$  all modes with  $m \neq \pm 1$  give no contribution to the integral (26) due to the angular symmetry, and the soliton velocity results as follows

$$\frac{d\mathbf{X}}{dt} = \frac{i\omega_0 l_0 N_0}{2N} (C_{-1} e^{i\omega_{-1}t} - C_1 e^{i\omega_1 t}), \quad (28)$$

where the constants  $C_m$  are determined by the static soliton structure,

$$C_m = A_m \int_0^\infty d\rho \left\{ \rho \sin^2 \theta_0(\rho) \left[ \frac{g_m(\rho)}{\sin \theta_0(\rho)} \right]' + g_m(\rho) \sin \theta_0(\rho) + m f_m(\rho) \sin 2\theta_0(\rho) \right\}. \quad (29)$$

The mode with  $m = 1$  is the zero-frequency local mode, which describes a shift of the soliton position, its eigenspectrum has the form [31]

$$f_1(\rho) = \theta_0'(\rho), \quad g_1(\rho) = -\frac{\sin \theta_0(\rho)}{\rho}, \quad \omega_1 = 0.$$

A simple calculation shows that  $C_1 = 0$ , therefore the soliton motion is connected only with the mode  $m = -1$ ,

$$\mathbf{X}(t) = R_{\text{orb}} e^{-i\omega_{-1}t}, \quad R_{\text{orb}} = \frac{|C_{-1}| N_0 \omega_0 l_0}{2N\omega_{-1}}. \quad (30)$$

Thus, only the perturbation with the symmetry of the mode  $m = -1$  can lead to a soliton motion as a whole. As we have found, the best way to excite such a mode is to use the exact shape of this mode, calculated in linear approximation, with *finite* amplitude of deformation  $A_{-1}$ . We will check this prediction in Sec. 7.

## 6. Numerical Simulations for the Circular Symmetric Topological Precessional Soliton

To validate predictions of the continuum theory for the soliton properties, we integrate numerically the discrete Landau–Lifshitz equations (2) over square lattices of size  $(2L)^2$  using a 4th-order Runge–Kutta scheme with time step 0.01. Each lattice is quadratic with the length  $L$ . We use periodic boundary conditions:

$$\begin{aligned} \text{left border} \quad \mathbf{S}(0, 0 \dots L+a) &= \mathbf{S}(L, 0 \dots L+a) \\ \text{right border} \quad \mathbf{S}(L+a, 0 \dots L+a) &= \mathbf{S}(a, 0 \dots L+a) \\ \text{lower border} \quad \mathbf{S}(0 \dots L+a, 0) &= \mathbf{S}(0 \dots L+a, L) \\ \text{upper border} \quad \mathbf{S}(0 \dots L+a, L+a) &= \mathbf{S}(0 \dots L+a, a). \end{aligned}$$

In all cases the soliton is started near the center of the domain. We have fixed the exchange constant  $J = \hbar = 1$  as well as the spin length  $S = 1$ . We have considered the anisotropy parameter in the range  $\delta \in (0.0005; 0.1)$ , corresponding to  $l_0/a \in (22.4, 1.58)$  so that we are close to the continuum limit. We consider system sizes in the range  $L/a \in (50, 800)$ .

We start the simulations using an initial soliton-like distribution

$$\theta = \theta_0(r), \quad \phi = \varphi_0 + \chi, \quad (31)$$

with the trial function (23) for the  $\theta$ -field. Evidently, the soliton solutions of the Landau–Lifshitz equations for a lattice differ from the circular symmetric continuous solutions, and also from the simple trial function. To find such a “pure” soliton solution, i.e. to adapt the trial solution to the lattice, one should provide enough time for the decay of the initial error in the trial functions. In fact, using (31) as

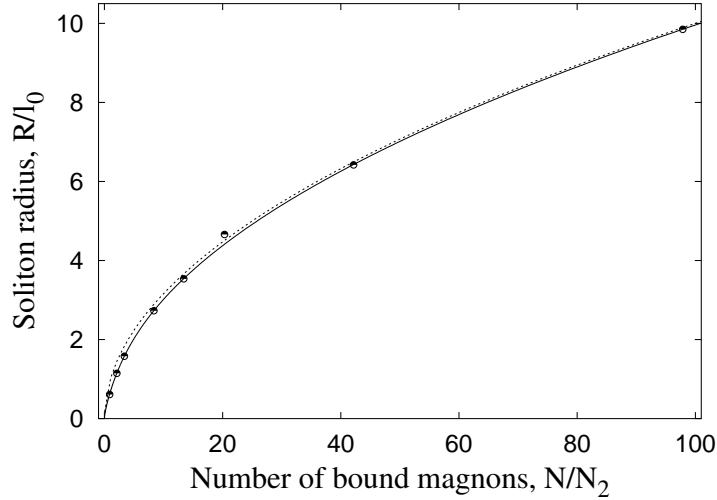


**Figure 1.** Radius of the soliton as a function of the number of bound magnons. The symbols correspond to the simulation data; the solid line is the result of continuum model integration; the dashed line corresponds to Eq. (34)

initial conditions for the lattice we excite also magnons, which should be taken out the system. To avoid the problem of magnons we have damped them the initial stage of simulations by applying damping. This kills all spreading spin waves coming from the imperfect initial condition. In this way instead of Eqs. (2), we have integrated numerically Landau–Lifshitz equations with Gilbert damping

$$\hbar(1 + \varepsilon^2) \frac{d\mathbf{S}_n}{dt} = - \left[ \mathbf{S}_n \times \frac{\partial \mathcal{H}}{\partial \mathbf{S}_n} \right] + \frac{\varepsilon}{S} \left[ \mathbf{S}_n \times \left[ \mathbf{S}_n \times \frac{\partial \mathcal{H}}{\partial \mathbf{S}_n} \right] \right], \quad (32)$$

see Ref. [44] for details. The lowest frequency of the continuous magnon spectrum is  $\omega_0$ , thus the damping time  $t_d \approx 1/(\varepsilon\omega_0)$ , see Ref. [32] for details. During the damping time ( $t < t_d$ ), the magnons are damped in the system, but the soliton is also damped, and the soliton energy  $\mathcal{E}$  decays as well as the number of bound magnons  $N$ . In order to save the soliton structure, we should switch off the damping before we damp out the soliton, i.e.  $t < 1/\varepsilon\omega_p$ . In all simulations we use the same value of  $\varepsilon = 0.02$ , then the damping time  $t_d \approx 12/\delta$ , and the damping is turned off *adiabatically* after a time greater than  $t_d$ .

Let us discuss the choice of the other parameters. In all simulations we want to be not far from the continuum limit in order to validate the theory. It means that the magnetic length  $l_0$  should be greater than the lattice constant  $a$ . This regulates the choice of the anisotropy constant  $\delta = a^2/4l_0^2$ . Besides  $l_0$  the soliton solution has two extra parameters:  $R$ , which is the soliton radius, and  $r_0$ , which characterizes the scale of the exponential decay of the excitation far from the soliton center.

We start with the large radius solitons. In this case  $R \gg r_0 \approx l_0$ , and we can limit ourselves by choosing  $\delta = 0.1$  (this corresponds to  $l_0 \approx 1.5a$ ). The system size  $L$  should be much greater than the largest parameter of the soliton, which is its radius. We consider solitons up to the radius  $R = 20l_0 \approx 31.4a$ . Thus we consider lattices with  $L = 200a$ , which satisfy all above mentioned conditions.

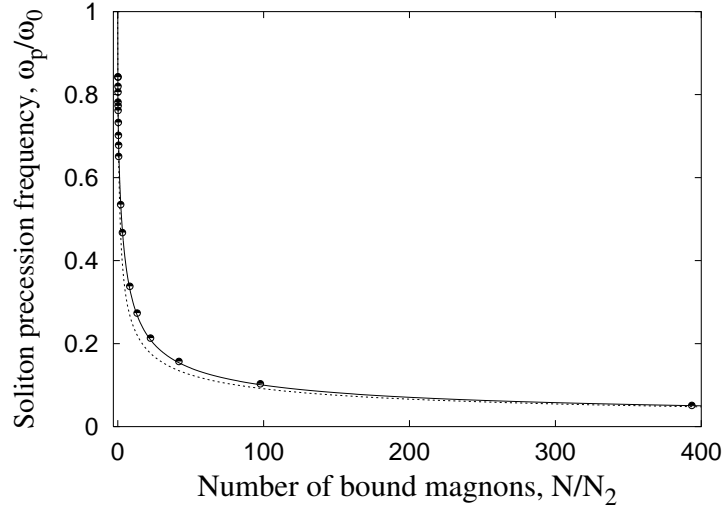


**Figure 2.** Soliton precession frequency as a function of the number of bound magnons. Symbols correspond to the simulation data; the solid line is the result of continuum model integration; the dashed line corresponds to Eq. (35).

In the case of small radius solitons we have the following relation between the parameters of the system:

$$a \ll R \ll l_0 \ll r_0 \ll L. \quad (33)$$

For the smallest soliton we choose  $\delta = 0.0005$ , which corresponds to  $l_0 \approx 22.4a$ ; this gives the possibility to consider solitons of small radii down to  $R = 0.225l_0 \approx 5a$ . However, such a small anisotropy drastically changes the soliton shape far from the center, which has the scale  $r_0$ , see Eq. (19). For example, for the soliton with  $R = 0.225l_0$ , the precession frequency  $\omega_p \approx 0.84\omega_0$  (see Ref. [31]), which results in  $r_0 = l_0/\sqrt{1 - \omega_p/\omega_0} \approx 56a$ . Thus to consider small radius solitons we must increase the system size. In our spin dynamics simulations we choose  $L = 800a$  for the smallest solitons. To perform simulations for such large systems,  $800 \times 800$ , we have used parallelize a computations, see Appendix A.

Let us discuss results of our spin dynamics simulations. Starting from initial conditions (31), and adapting the soliton shape to the lattice, we have obtained the class of one-parameter stable soliton solutions for a wide range of the parameter  $N$ , or equivalently, the soliton radius  $R$ . We have studied the  $R(N)$  dependence, which is presented in Fig. 1. Almost in the full range of parameters, the simple dependence

$$N \approx N_0 \left( \frac{R}{l_0} \right)^2 \quad (34)$$

is valid. Note that the dependence (34) was verified numerically in Ref. [32] for the large radius solitons only, where  $R > 10l_0$ . Here we want to check the continuum results for arbitrary  $R$ . Using (22) and (34), an approximate dependence

$$\omega_p(N) \approx \frac{\omega_0}{1 + \sqrt{N/N_0}} \quad (35)$$

can be derived. One can see from Fig. 2 that this simple dependence works well in a wide range of parameters.

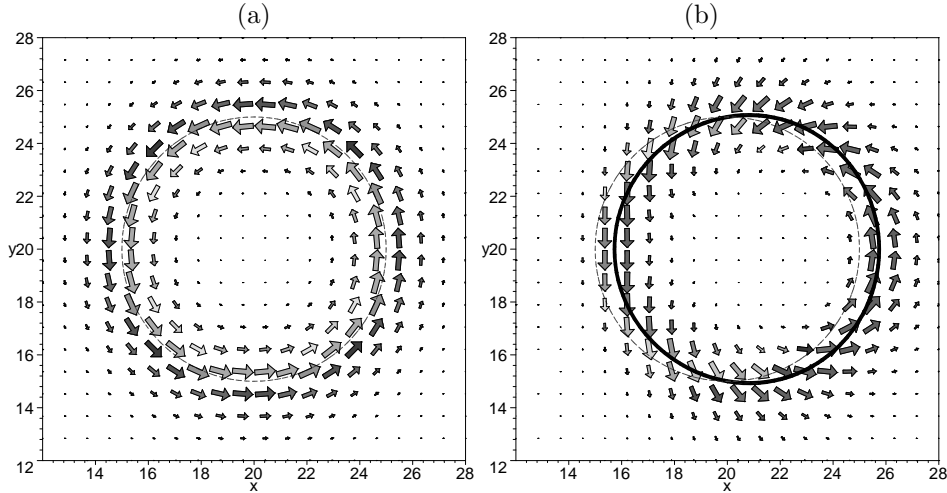


**Figure 3.** In-plane spin distribution for the soliton with  $R = 5l_0$ . Fig.(a) corresponds to the circular symmetric soliton and (b) to an elliptically deformed one. The lines describe the contour plot of  $S_z = 0$  ( $\theta = \pi/2$ ): the dashed line is for the circular symmetric soliton and the solid line is for the deformed soliton.

## 7. Simulation of the Soliton Motion

In the previous section we have performed spin dynamics simulations only for the circular symmetric precessional soliton, which does not move as a whole. As mentioned in Sec. 5, in order to move the soliton one should break its symmetry. We have done this by an initial deformation of the soliton shape, and integrated numerically the Landau–Lifshitz equations. Specifically, we have chosen an elliptical kind of deformation, which corresponds to the shape of the internal partial mode with azimuthal quantum number  $m = -1$ . We start the simulations with initial conditions

$$\theta = \theta_0(\rho) + Af(\rho) \cos \chi, \quad \phi = \varphi_0 + \chi - \frac{A}{\sin \theta_0} g(\rho) \sin \chi \quad (36)$$

by the same numerical scheme as described in the previous section. We calculated the functions  $f \equiv u_{-1} + v_{-1}$  and  $g \equiv u_{-1} - v_{-1}$  numerically solving the eigenvalue problem (27) by the two-parametric shooting scheme as described in Ref. [31]. The parameter  $A$  is the amplitude of the eigenmode, which characterizes the magnitude of the soliton deformation. An initial distribution of spins, which corresponds to Eqs. (36), is shown in Fig. 3 and can be seen to describe the elliptical kind of the soliton deformation.

During the simulations we have computed the time dependence of the position  $\mathbf{X}(t) = (X(t), Y(t))$  of the soliton center:

$$\mathbf{X}(t) = \frac{\sum_{\mathbf{n}} \mathbf{r}_{\mathbf{n}} [S - S_{\mathbf{n}}^z(t)]}{\sum_{\mathbf{n}} S - S_{\mathbf{n}}^z(t)}, \quad (37)$$

which is the discrete analogue of Eq. (24);  $\mathbf{r}_{\mathbf{n}} = (x_n, y_n)$  are the lattice points.

We have found numerically that after switching off the damping, the soliton reaches very fast a circular trajectory, see Fig. 4. This results in a nice circular motion with constant frequency. For small deformations the radius of the orbit is proportional to the initial deformation. One can say that the effect of a circular motion and the

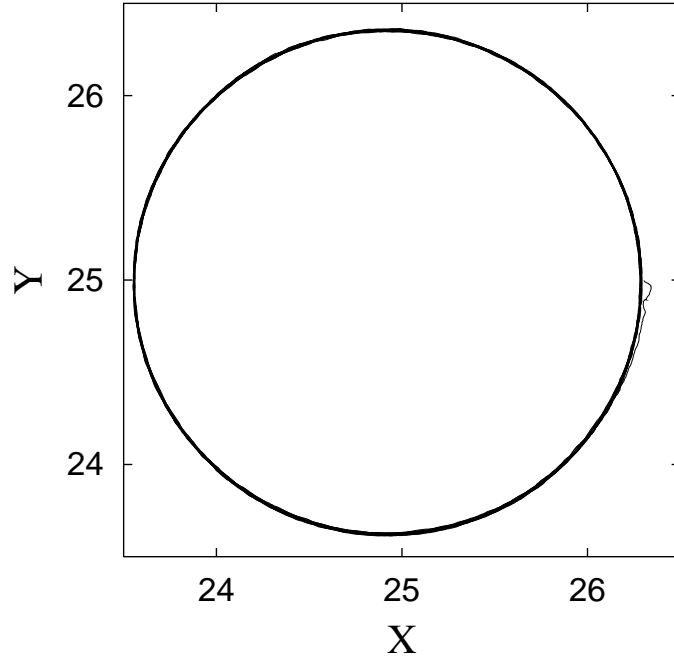


**Figure 4.** Trajectory of the soliton with initial radius  $R = 4.87l_0$  and initial precession frequency  $\omega_p = 0.2\omega_0$ .

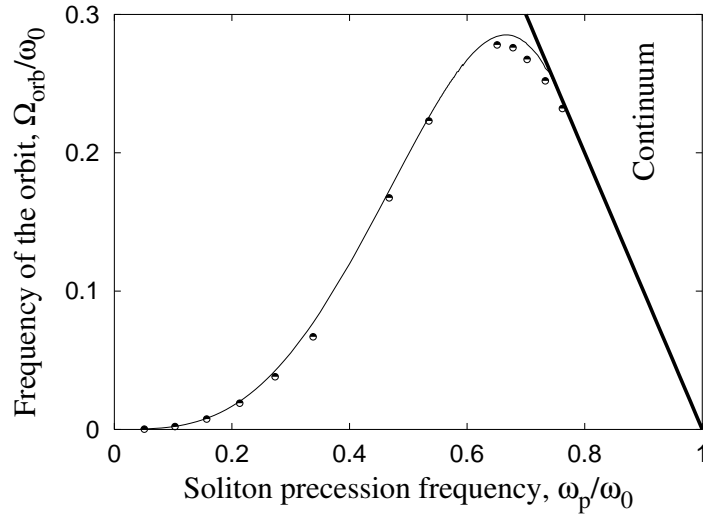


**Figure 5.** Frequency of the orbit motion as a function of the precession frequency of the soliton. Symbols correspond to the spin dynamics simulation data; lines corresponds to the frequency of the eigenmode with  $m = -1$  from the continuum theory by Sheka et al. [31].

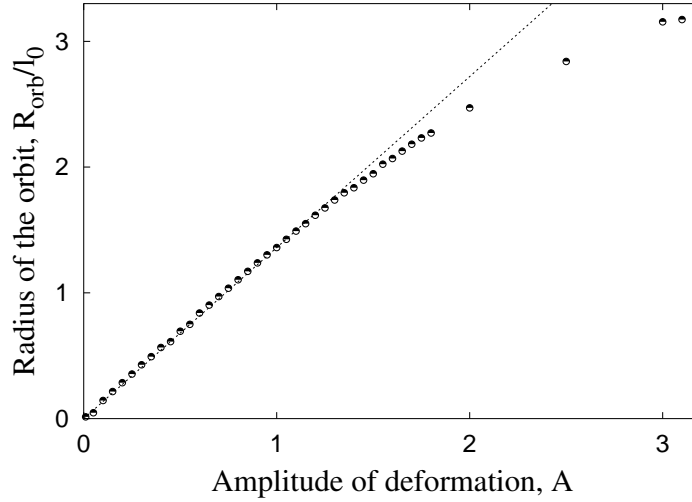


**Figure 6.** Radius of the soliton orbit as a function of the deformation amplitude  $A$ . Parameters of the soliton: initial radius  $R = 4.87l_0$  and initial precession frequency  $\omega_p = 0.2\omega_0$ .

excitation of the mode with  $m = -1$  are identical for this case, as predicted by Sheka et al. [31]. Such a relation is valid in some range of the soliton deformation for all soliton radii, see Fig. 5. Then, for larger deformations, non-linear regime is clearly seen, see Fig. 6. The frequency of this orbit motion of the soliton approximately corresponds to the frequency of the local mode,  $\Omega_{\text{orb}} = \omega_{m=-1}$ .

The presence of such an exact circular motion, with only one frequency, independent of the orbit radius (even in non-linear regime), gives the possibility to conclude that this is the *first* observation of the pure gyroscopic motion, which is equivalent to the Larmor precession of a charged particle in a magnetic field. Therefore, the soliton motion can be described by an effective equation of motion for the position of the soliton  $\mathbf{X}$ , which takes the form of usual Newtonian equation for a particle with the *well-defined effective mass*  $M$  under the influence of the gyroscopic force  $\mathbf{F}_g$ :

$$M \frac{d^2 \mathbf{X}}{dt^2} = \mathbf{F}_g, \quad \mathbf{F}_g = G \left[ \mathbf{e}_z \times \frac{d\mathbf{X}}{dt} \right]. \quad (38)$$

Here  $G = 4\pi\hbar S/a^2$  is the gyroconstant, see [1]. Formally, Eq. (38) has two solutions. One solution,  $\mathbf{X} = \text{const}$ , corresponds to the translation mode with  $m = +1$ . In the infinite system this is a zero-frequency local mode, which describes a simple shift of the soliton,  $\omega_{m=+1} = 0$ . The second solution describes a circular motion with the frequency  $\Omega_{\text{orb}} = G/M$ . Thus, we can calculate the effective mass of the soliton using the simulation data for the orbit frequency.

We have checked how the orbit frequency depends on the soliton radius. For the large radius solitons  $\Omega_{\text{orb}} \approx 2\omega_0(l_0/R)^3$  is in good agreement with the results for the local modes. For the small radius solitons, the orbit frequency tends to the boundary of the spectrum,  $\Omega_{\text{orb}} \approx \omega_0 - \omega_p$ . In the case  $N \ll N_0$  one can use the approximate limiting expression (20) for  $\omega_p$ , which results in  $\Omega_{\text{orb}} \approx \omega_0 / \ln(8N_0/e\gamma^2 N)$ . This

dependence corresponds to our result for the eigenfrequencies, see [31]. The frequency tends to zero when  $R \rightarrow 0$ .

One can calculate the effective mass of the soliton by  $M = G/\Omega_{\text{orb}}$ ,

$$M = M_0 F\left(\frac{N}{N_0}\right), \quad M_0 = \frac{G}{\omega_0} = \frac{\pi \hbar^2}{J a^2 \delta}, \quad (39)$$

where  $M_0$  is a characteristic value of the effective mass, found in Ref. [30]. The function  $F(\bullet) = \omega_0/\Omega_{\text{orb}}(\bullet)$  depends on the soliton size having the asymptotic behavior

$$F(x) = \begin{cases} \ln\left(\frac{8}{e\gamma x}\right), & \text{when } x \ll 1 \\ \frac{1}{2}x^{3/2}, & \text{when } x \gg 1 \end{cases}. \quad (40)$$

The soliton mass diverges in the limiting cases when  $R \rightarrow 0$  and  $R \rightarrow \infty$ . Note that for the large radius solitons the mass increases faster than the domain wall width, which is proportional to  $R$ . The mass takes a minimum value  $M_c \approx 3.51M_0$  for the soliton with  $R_c \approx 0.547l_0$ . The soliton with these parameters has the highest *mobility*.

## 8. Conclusion

In this paper we have studied the dynamics of topological solitons in classical 2D easy-axis ferromagnet. The analysis was made both analytically in the continuum approximation and numerically using the spin dynamics simulations for a wide range of solitons: from large radius solitons to small ones. Our simulations were performed for small anisotropies, which corresponds to the continuum description. We have checked and confirmed a number of results from the continuum theory about the soliton structure, in particular, the connection between the number of bound magnons and the precession frequency of the spins inside the soliton.

The main issue is connected with the soliton dynamics. We have proposed a way how to move a soliton exciting one of its internal modes. To our knowledge, it is the first observation of inertial motion of 2D magnetic solitons. The effective soliton dynamics is similar to the Larmor dynamics of a charged particle in a magnetic field. By analysis of the effective soliton dynamics we extract information about the effective mass of the soliton. This mass essentially depends on the anisotropy,  $M \propto 1/\delta$ , and on the soliton size, having the minimum for the soliton of the size about  $0.5l_0$ . In the case of large radius solitons the soliton mass increases with the increase of the soliton radius. Note that it increases faster than the number of the bound magnons,  $M \approx \frac{1}{2}M_0(N/N_0)^{3/2}$ . Such dependence is in a good agreement with previous results [30]; the soliton mass diverges in the limit case  $R \rightarrow \infty$ , which corresponds to the fact that the single domain wall can not move. When the soliton radius is smaller, the effective mass increases logarithmically with its radius, and diverges in the limit case  $R = 0$ . Note that the problem of inertial properties of a small radius soliton have caused a lot of discussions. According to linear analysis [30], the soliton mass tends to some limit value  $M^* = 6\sqrt{\pi}(\pi + 2)M_0 \approx 55M_0$  when  $R \rightarrow 0$ . At the same time our previous analysis of eigenmodes [31] shows that  $M \rightarrow \infty$  at the limit case  $R \rightarrow 0$ . Spin dynamics simulations confirm our results on internal modes: the soliton loses its mobility when becomes very small.

We have predicted the fine circular motion of the soliton by exciting its internal mode. We believe that such phenomenon can be observed experimentally, e.g. by ac

pumping. Our investigations can be important also for the quantum Hall systems, where skyrmion-type solitons are well-known to lead to the breakdown of the spin-polarized quantum Hall effect [45].

### Acknowledgments

D. D. Sheka thanks the University of Bayreuth, where part of this work was performed, for kind hospitality and acknowledges support from Deutsches Zentrum für Luft- und Raumfahrt e.V., Internationales Büro des Bundesministeriums für Forschung und Technologie, Bonn, in the frame of a bilateral scientific cooperation between Ukraine and Germany, project No. UKR-02-011. D. D. Sheka acknowledge also the support from Ukrainian-French “Dnipro” grant (No. 09855WF). C. Schuster thanks Stefan Karpitschka for his kind support concerning aspects of parallelizing the source code.

### Appendix A. Parallelized Computations

There exist two main possibilities of parallelization computations: (i) the usage of a vector-computing machine which has a shared memory or (ii) the usage of a cluster system (usually a Linux cluster) with communication between the different processors (nodes). The latter process is called *message passing interface* (MPI), this interface does not depend on the programming language.

In MPI there is a master-process which is responsible for the administration of the data, i.e. initializations, reading or saving of data, whereas the other nodes (slaves) are doing the calculation (e.g. integration). In our case we divide the lattice into horizontal stripes. As in our system we take into account nearest-neighbor interaction we must put a communication between the borders of the stripes. To make calculations for the  $i$ -th stripe we need the lower border of the  $(i + 1)$ -th stripe and the upper boarder of the  $(i - 1)$ -th stripe. This exchange is done after every second integration step in the Runge Kutta algorithm. This advantages a good equilibrium between the latency period (time in which the nodes are synchronized), data-transferring time, and calculation time. As the boundary condition of our lattice is periodic the upper boarder of the top stripe is exchanged with the lower border of the bottom stripe. Concerning the left and right boarders of one stripe there are no communication processes, because horizontal cuts of the system advantage an internal exchange of the lateral borders in one process.

As the data is always transferred between the same nodes we implement a *persistant connection mode* in order to make the *overhead* (additional time spent on the connection establishment) smaller. Theses connections are built up at the beginning of the integration to be ready for a fast use.

The transfer takes place in an asynchronous, buffered mode. Thereby the data resulting of the calculation on a stripe is put into a buffer so that for this node there is no need to wait until the other nodes are ready to receive. In order to do a new calculation in the next time steps the stripe awaits information of its neighbored stripes. The advantage of this method is that the time exposure for the synchronization of the nodes decreases.

After integrating 40 time steps with  $\Delta t = 0.01$  we calculate the soliton position  $\mathbf{X}(t)$  discretely and optimally distributed over the other nodes. After finishing the calculations the data is sent from the slaves to the master-process which saves the data in a file.



The simulation is interrupted as soon as the master-process finds in the working directory a file which we arbitrarily call "VMDCANCEL". But before the simulation stops all spin data are sent to the master-process which writes the complete spin-field into a file. This advantages the simulation to continue from this last time step anytime later.

The parallelizing of the source code is much easier and more effective if one can use shared memory multi-processors machines. The loops are environed by sunstyle parallelization-directives. According to the dependency of the variables they have to be declared as *private variables* and others as *reduction variables*. *Private variables* take different values in different threads (such as auxiliary variables) so there is no shared memory for these variables. *Reduction variables* are used for sums which are distributed over different threads during one loop and are added in the end of the parallelized loop. The advantage of this method is a very fast access to the shared memory of all threads. This avoids a time consuming latency period caused by a communication process. To summarize we want to stress that a shared memory machine is always much faster than a cluster, if one considers a fixed number of processors to be in use. The only advantage a cluster has is the fact that compared to a shared memory machine it has much more processors and the number of processors can be increased arbitrarily. Also aspects of the price motivate universities and institutes to buy a cluster instead of a shared memory machine.

## References

- [1] A. M. Kosevich, B. A. Ivanov, and A. S. Kovalev, Phys. Rep. **194**, 117 (1990).
- [2] V. G. Bar'yakhtar, M. V. Chetkin, B. A. Ivanov, and S. N. Gadetskii, *Dynamics of Topological Magnetic Solitons. Experiment and Theory* (Springer-Verlag, Berlin, 1994).
- [3] F. G. Mertens and A. R. Bishop, in *Nonlinear Science at the Dawn of the 21th Century*, edited by P. L. Christiansen, M. P. Soerensen, and A. C. Scott (Springer-Verlag, Berlin, 2000).
- [4] V. L. Berezinskiĭ, Sov. Phys JETP **34**, 610 (1972).
- [5] J. M. Kosterlitz and D. J. Thouless, J. Phys. **C 6**, 1181 (1973).
- [6] F. G. Mertens, A. R. Bishop, G. M. Wysin, and C. Kawabata, Phys. Rev. **B 39**, 591 (1989).
- [7] L. P. Regnault, J. P. Boucher, J. Rossat-Mignod, J. Bouillot, R. Pynn, J. Y. Henry, and J. P. Renard, Physica **B+C 136**, 329 (1986).
- [8] M. T. Hutchings, P. Day, E. Janke, and R. Pynn, J. Magn. Magn. Mater. **54–57**, 673 (1986).
- [9] S. T. Bramwell, M. T. Hutchings, J. N. J, R. Pynn, and P. Day, J. de Phys. **49 (C-8)**, 1435 (1988).
- [10] D. D. Wiesler, H. Zabel, and S. M. Shapiro, Physica **B 156–157**, 292 (1989).
- [11] L. P. Regnault and J. Rossat-Mignod, *Magnetic Properties of Layered Transition Metal Compounds* (Kluwer Academic, 1990).
- [12] A. A. Belavin and A. M. Polyakov, JETP Lett. **22**, 245 (1975).
- [13] F. Waldner, J. Magn. Magn. Mater. **31—34**, 1203 (1983).
- [14] F. Waldner, J. Magn. Magn. Mater. **54—57**, 873 (1986).

- [15] F. Waldner, *J. Magn. Magn. Mater.* **104—107**, 793 (1992).
- [16] C. E. Zaspel, *Phys. Rev.* **B 48**, 926 (1993).
- [17] C. E. Zaspel, T. E. Grigereit, and J. E. Drumheller, *Phys. Rev. Lett.* **74**, 4539 (1995).
- [18] C. E. Zaspel and J. E. Drumheller, *International Journal of Modern Physics* **10**, 3649 (1996).
- [19] R. H. Hobard, *Proc. Phys. Soc.* **82**, 201 (1963).
- [20] G. H. Derrick, *J. Math. Phys.* **5**, 1252 (1964).
- [21] V. G. Bar'yakhtar and B. A. Ivanov, *Sov. Sci. Rev. Sec.A.* **16**, 3 (1993).
- [22] B. A. Ivanov, *JETP Lett.* **56**, 118 (1992).
- [23] A. A. Zhmudskii and B. A. Ivanov, *JETP Lett.* **65**, 945 (1997).
- [24] S. R. Coleman, *Nucl. Phys.* **B 262**, 263 (1985).
- [25] T. D. Lee and Y. Pang, *Phys. Rept.* **221**, 251 (1992).
- [26] R. A. Battye and P. M. Sutcliffe, *Nuclear Physics* **B 590**, 329 (2000).
- [27] V. G. Makhankov, *Phys. Rep.* **35**, 1 (1978).
- [28] B. A. Ivanov, H. J. Schnitzer, F. G. Mertens, and G. M. Wysin, *Phys. Rev.* **B 58**, 8464 (1998).
- [29] N. Papanicolaou and W. J. Zakrzewski, *Physica* **D 80**, 225 (1995).
- [30] B. A. Ivanov and V. A. Stephanovich, *Phys. Lett.* **A 141**, 89 (1989).
- [31] D. D. Sheka, B. A. Ivanov, and F. G. Mertens, *Phys. Rev.* **B 64**, 024432 (2001).
- [32] T. Kampeter, S. A. Leonel, F. G. Mertens, M. E. Gouvêa, A. S. T. Pires, and A. S. Kovalev, *Eur. Phys. J.* **B 21**, 93 (2001).
- [33] H. Walliser and G. Holzwarth, *Phys. Rev.* **B 61**, 2819 (2000).
- [34] R. E. Prange and S. M. Girvin, eds., *The quantum Hall effect* (Springer, New York, 1990).
- [35] S. L. Sondhi, A. Karlhede, S. A. Kivelson, and E. H. Rezayi, *Phys. Rev.* **B 47**, 16419 (1993).
- [36] T. H. Skirm, *Proc. R. Soc. London* **A 260**, 127 (1961).
- [37] R. H. Hobard, *Proc. Phys. Soc.* **85**, 610 (1965).
- [38] U. Enz, *J. Math. Phys.* **18**, 347 (1977).
- [39] U. Enz, *J. Math. Phys.* **19**, 1304 (1978).
- [40] A. S. Kovalev, A. M. Kosevich, and K. V. Maslov, *JETP Lett* **30**, 296 (1979).
- [41] A. M. Kosevich and V. P. Voronov, *Sov. J. Low Temp. Phys.* **7**, 442 (1981).
- [42] V. P. Voronov, B. A. Ivanov, and A. K. Kosevich, *Sov. Phys JETP* **84**, 2235 (1983).
- [43] B. A. Ivanov and V. A. Stephanovich, *Sov. Phys JETP* **64**, 376 (1986).
- [44] D. D. Sheka, J. P. Zagorodny, J. G. Caputo, Y. Gaididei, and F. G. Mertens, *Phys. Rev.* **B 71**, 134420 (2005).
- [45] N. R. Cooper, *Phys. Rev. Lett.* **80**, 4554 (1998).